Performance Analysis and Comparison of Two Fault-Tolerant Model Predictive Control Methods for Five-Phase PMSM Drives

Wentao Huang, *Member*, *IEEE*, Wei Hua, *Senior Member*, *IEEE*, Qigao Fan, *Member*, *IEEE*

***Abstract*—Model predictive current control (MPCC) and model predictive torque control (MPTC) are two derivatives of model predictive control. These two control methods have demonstrated their strengths in the fault-tolerant control of multiphase motor drives. To explore the inherent link, the pros and cons of two strategies, the performance analysis and comparative investigation of MPCC and MPTC are conducted through a five-phase permanent magnet synchronous motor with open-phase fault. In MPCC, the currents of fundamental and harmonic subspaces are simultaneously employed and constrained for a combined regulation of the open-circuit fault drive. In MPTC, apart from the torque and the stator flux related to fundamental subspace, the *x-y* currents are also considered and predicted to achieve the control of harmonic subspace. The principles of two methods are demonstrated in detail and the link is explored in terms of the cost function. Besides, the performance by two methods is experimentally assessed in terms of steady-state, transition, and dynamic tests. Finally, the advantages and disadvantages of each method are concluded.**

***Index Terms*—Permanent magnet motor, five-phase, fault-tolerant control, model predictive control.**

I. Introduction

MULTI-PHASE motor drives have been increasingly gaining attention in many industrial applications with high reliability requirements due to their remarkable fault tolerance [1]-[2]. Extensive research has been conducted to improve the fault-tolerant ability and performance of multi-phase drives under different faulty conditions [3]-[6].

Among all types of failures, the most widely studied is open-circuit fault (OCF) in recent years. In order to obtain an undisturbed rotating magneto-motive force (MMF) after OCF, control strategies, including maximum torque (MT) and minimum loss (ML), are proposed based on the demands of actual applications [6]. With these criteria, the classic field-oriented control (FOC) and direct torque control (DTC), which are popularly used for motor drives under healthy conditions, have been investigated in the field of multi-phase drives under faulty situations. Both hysteresis comparator and pulse width modulation (PWM) are utilized to generate pulse patterns in fault-tolerant FOC [7]-[9] and DTC [10]-[13] schemes. The employment of PWM can achieve superior steady-state performance and constant switching frequency compared with hysteresis regulators. Generally, the transient behaviors of DTC are more desirable since the stator flux amplitude and torque are directly controlled. Different from normal healthy operations, the fundamental and harmonic components under OCF situations become coupled with a decrease of the control degree of freedom. Hence, the joint regulation of both subspaces should be considered. With the development of vector space decomposition (VSD), an extra proportional-integrator (PI) or proportional-resonant (PR) controller is usually employed in fault-tolerant FOC [7] and fault-tolerant DTC [13] to realize control of harmonic subspace.

Recently, the model predictive control (MPC) has become a significant alternative for high performance control of motor drives. According to the control variable, MPC can be categorized into two sorts, model predictive current control (MPCC) [14]-[16] and model predictive torque control (MPTC) [18]-[20]. When MPC strategy is applied in multi-phase motor drives in faulty states, the regulations of both fundamental and harmonic subspaces can be obtained by designing predictive models and optimizing cost functions. Unlike the structures of fault-tolerant FOC and DTC, no extra controller or control loop is required when MPC is applied. In [21], the MPCC method is explored on a five-phase induction motor (IM) drive under the open-phase situation. The predictive model and cost function associated with the current components in the *x-y* subspace are constructed for complete control of the faulty drive. In [22]-[23], the MPCC approach is utilized to enhance the fault-tolerant performance of six-phase permanent magnet synchronous motor (PMSM) drives under OCF conditions. Compared to fault-tolerant MPCC, research on MPTC is relatively rare. Derived from the classic hysteresis-based DTC, the fault-tolerant MPTC is also concentrated on the regulation of the torque and stator flux amplitude, which are both related to the α-β subspace. In [24], the MPTC schemes are developed to realize independent control of different motors in multi-motor drives under OCF operation. Later, the harmonic regulation has been considered in fault-tolerant MPTC of five-phase PMSM drives [25]-[26]. The predictive model of the *x-y* current is built and taken into account during the cost function optimization. As a result, complete control of the faulty five-phase drive is achieved.

Manuscript received May 09, 2021; revised June 18, 2021; accepted July 06, 2021. date of publication December 25, 2021; date of current version December 18, 2021.

This work was supported in part by the Fundamental Research Funds for Central Universities under Grant JUSRP121020, the Natural Science Foundation of Jiangsu Province under Grant BK20210475

W. Huang and Q. Fan are with the School of Internet of Things Engineering, Jiangnan University, Wuxi, 214122, China (e-mail: wentao.h@jiangnan.edu.cn, qgfan@jiangnan.edu.cn)

W. Hua is with the School of Electrical Engineering, Southeast University, Nanjing 210096, China (e-mail: huawei1978@seu.edu.cn).

(Corresponding Author: Wei Hua)

Digital Object Identifier 10.30941/CESTEMS.2021.00036

Comparative studies have been carried out to explore differences and similarities of fault-tolerant performance by different control schemes. In [21], a quantitative comparison between FOC with the proportional integral-resonant controller and MPCC has been conducted with both MT and ML methods. It is found that MPCC can provide faster control response and superior performance at low-speed operation but at the expense of higher current ripples. Later, the performances by MPCC, PR-based DTC and FOC have been experimentally evaluated in terms of steady-state and dynamic conditions for a five-phase IM with OCF [27]. The results indicate that the change of control structure after OCF is minimum when MPCC is used.

Generally, most of the research is focused on the performance analysis and comparison between MPCC and classic linear control strategy for multi-phase drives under OCF operation. Although behaviors of MPCC and MPTC are assessed experimentally for three-phase IM drives [28]-[29] and a PMSM fed by a matrix converter [30] under normal operation, the inherent relationship between two control strategies has not been disclosed. Moreover, fault-tolerant MPCC and MPTC have not been comparatively evaluated for multi-phase motor drives with OCF.

Hence, this paper presents a comprehensive comparison of fault-tolerant MPCC and MPTC for a five-phase PMSM drive with OCF. For the simultaneous regulations of fundamental and harmonic subspaces, the currents of two subspaces are employed and constrained in MPCC. Apart from the torque and stator flux, the *x*-*y* currents are additionally considered to achieve the control of harmonic subspace in MPTC. The principles of two methods are demonstrated in detail and the inherent link is explored through cost functions. Besides, the performance by two methods is experimentally assessed in terms of steady-state, transition, and dynamic tests. Finally, the advantages and disadvantages of each method are concluded. This work provides an effective principle for the proper selection of MPC methods in practical engineering applications.

The remainder of this paper is organized as follows: The modeling of a five-phase PMSM drive under OCF conditions is introduced in Section II. The principles of fault-tolerant MPCC and MPTC methods are presented in Section III and Section IV, respectively. In Section V, the inherent relationship is investigated and discussed. The performances by two fault-tolerant MPC strategies are evaluated by simulations and experiments in Sections VI and VII, respectively. The conclusions are presented in the final section.

II. Modeling of a Five-Phase PMSM Drive under OCF

Fig. 1 illustrates a conventional two-level voltage source inverter-fed five-phase PMSM drive. When two OCF occurs, e.g., phase A, the number of switching states decreases from 32 to 16 naturally, and consequently, the current of phase A, i_A will be zero. According to the available switching states, the remained healthy four-phase voltages are derived as

$$\begin{bmatrix} v_B \\ v_C \\ v_D \\ v_E \end{bmatrix} = \frac{U_{dc}}{4} \begin{bmatrix} 3 & -1 & -1 & -1 \\ -1 & 3 & -1 & -1 \\ -1 & -1 & 3 & -1 \\ -1 & -1 & -1 & 3 \end{bmatrix} \begin{bmatrix} S_B \\ S_C \\ S_D \\ S_E \end{bmatrix} \tag{1}$$

where U_{dc} is the DC power supply; S_n=1 when the upper switch of each inverter leg is ON, and S_n=0 when the upper switch is OFF (n=B, C, D, E).

Based on the theory of VSD, the four-phase voltages can be mapped into the α-β subspace and x-y subspaces, as illustrated in Fig. 2. Different from the healthy condition, here each space plane in the faulty state is unevenly divided into 12 sectors. In addition, the voltage vector magnitudes are classified into 6 types: 0, 0.145U_{dc}, 0.325U_{dc}, 0.441U_{dc}, 0.447U_{dc}, 0.616U_{dc}.

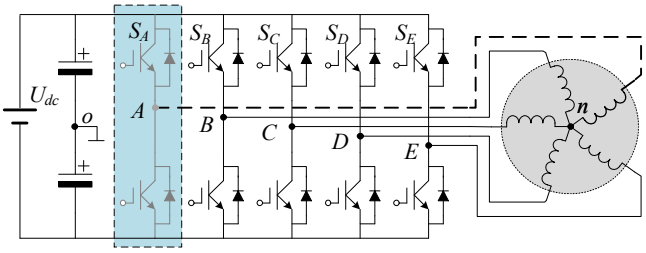

Fig. 1 Configurations of a five-phase PMSM drive under OCF condition.

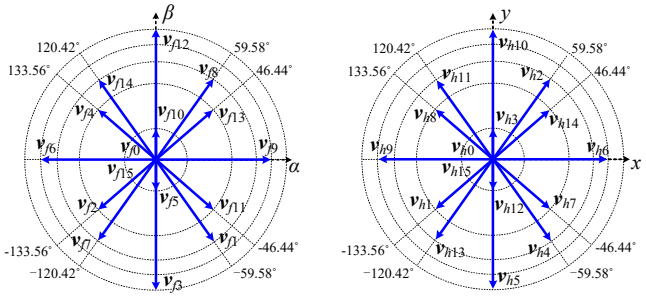

(a) (b)

Fig. 2 Voltage vectors in two subspaces. (a) α-β subspace. (b) x-y subspace.

Due to an OCF, the control degrees of freedom decrease. The amplitudes of the x-component and α-component currents are identical but the phase-angles are opposite. Consequently, only $\alpha\beta$-component and y-component currents are controllable in faulty drives. A modified VSD transformation is used to map the five-phase variables into the fundamental and harmonic subspaces as

$$T_C = \frac{2}{5} \begin{bmatrix} \cos\delta & \cos 2\delta & \cos 3\delta & \cos 4\delta \\ \sin\delta & \sin 2\delta & \sin 3\delta & \sin 4\delta \\ \sin 3\delta & \sin\delta & \sin 4\delta & \sin 2\delta \\ 1 & 1 & 1 & 1 \end{bmatrix} \tag{2}$$

where $\delta = 2\pi/5$.

With the extended Park transformation in (3), the voltage components in stationary coordinates are transformed to the d_1-q_1 and d_3-q_3 planes voltage components, respectively.

$$T_P = \begin{bmatrix} \cos\theta & \sin\theta & 0 & 0 \\ -\sin\theta & \cos\theta & 0 & 0 \\ 0 & 0 & \cos 3\theta & \sin 3\theta \\ 0 & 0 & -\sin 3\theta & \cos 3\theta \end{bmatrix} \tag{3}$$

where θ is the electrical rotor position.

Although the five-phase PMSM drive with OCF becomes an asymmetrical four-phase system, the mathematical model is similar to that under healthy operations. Neglecting the influence of flux-linkage harmonics, the voltage equations in the d_1-q_1-d_3-q_3 reference frame are given as [4]

$$\begin{cases} v_{d1} = R_S i_{d1} + L_{d1}\mathrm{d}i_{d1}/\mathrm{d}t - \omega_e L_{q1}\mathrm{d}i_{q1} \\ v_{q1} = R_S i_{q1} + L_{q1}\mathrm{d}i_{q1}/\mathrm{d}t + \omega_e\left(L_{d1}\mathrm{d}i_{d1} + \psi_f\right) \\ v_{d3} = R_S i_{d3} + L_{d3}\mathrm{d}i_{d3}/\mathrm{d}t - 3\omega_e L_{q3}\mathrm{d}i_{q3} \\ v_{q3} = R_S i_{q3} + L_{q3}\mathrm{d}i_{q3}/\mathrm{d}t + 3\omega_e L_{d3}\mathrm{d}i_{d3} \end{cases} \quad (4)$$

where v_{dm}, v_{qm}, i_{dm}, i_{qm}, and L_{dm} and L_{qm} are the d_m-q_m components of the phase voltages, currents, and inductances components, respectively; m={1, 3}; R_s is the stator resistance; ψ_f is the fundamental magnitude of phase PM flux-linkage; ω_e is the electrical angular frequency.

Accordingly, the equations of the stator flux-linkage and the electromagnetic torque can be expressed as

$$\begin{bmatrix} \psi_{sd} \\ \psi_{sq} \end{bmatrix} = \begin{bmatrix} L_{d1} & 0 \\ 0 & L_{q1} \end{bmatrix}\begin{bmatrix} i_{d1} \\ i_{q1} \end{bmatrix} + \begin{bmatrix} \psi_f \\ 0 \end{bmatrix} \quad (5)$$

$$T_e = \frac{5}{2}P_r\left[\psi_f i_{q1} + \left(L_{d1} - L_{q1}\right)i_{d1}i_{q1} + 3\left(L_{d3} - L_{q3}\right)i_{d3}i_{q3}\right] \quad (6)$$

where ψ_{sd} and ψ_{sq} are the stator flux-linkage components in the d_1-q_1 reference frame; P_r is the number of pole pairs.

III. MPCC FOR A FIVE-PHASE PMSM UNDER OCF CONDITION

For complete control of the faulty drive system, the simultaneous regulation of the fundamental and harmonic subspaces should be considered. Hence, the currents in two subspaces are employed as the control variables of the MPCC method. Fig. 3 illustrates the control diagram of the fault-tolerant MPCC of a five-phase PMSM under OCF.

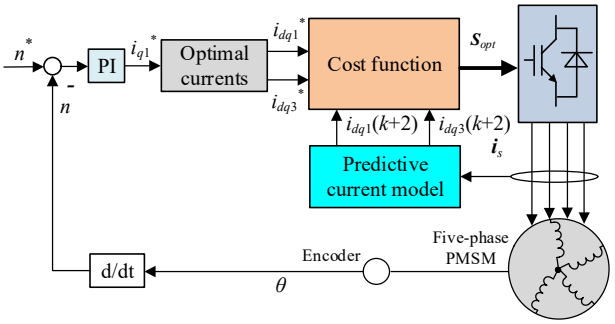

Fig. 3 Control diagram of fault-tolerant MPCC strategy for a five-phase PMSM under OCF condition.

A. Predictive Current Model

In a real digital implementation, there is a one-step delay between the obtained voltage vector and the applied vector. Therefore, a two-step prediction is used to compensate for the time delay. Using Euler's formula to discretize the voltage equation, the predictive current models are designed in the d_1-q_1-d_3-q_3 reference frame as

where $(k+1)$ and $(k+2)$ means the $(k+1)^{th}$ and $(k+2)^{th}$ sampling step, respectively, and T_s is the sampling time.

$$\begin{cases} i_{d1}(k+2) = \left(1 - R_s T_s / L_{d1}\right)i_{d1}(k+1) + w_e T_s L_{q1} i_{q1}(k+1)/L_{d1} + T_s v_{d1}/L_{d1} \\ i_{q1}(k+2) = \left(1 - R_s T_s / L_{q1}\right)i_{q1}(k+1) - w_e T_s L_{d1} i_{d1}(k+1)/L_{q1} + T_s / L_{11}\left(v_{q1} - w_e\psi_f\right) \\ i_{d3}(k+2) = \left(1 - R_s T_s / L_{q1}\right)i_{d3}(k+1) + 3w_e T_s L_{q3} i_{q3}(k+1)/L_{d3} + T_s v_{d3}/L_{d3} \\ i_{q3}(k+2) = \left(1 - R_s T_s / L_{q3}\right)i_{q3}(k+1) - 3w_e T_s L_{d3} i_{d3}(k+1)/L_{q3} + T_s v_{q3}/L_{q3} \end{cases} \quad (7)$$

B. Cost Function

Based on the predictive current model in (7), a cost function is subsequently designed to evaluate the optimal switching state in a manner where the absolute errors between the referenced and predicted currents are employed as

$$\begin{aligned} c_i = &\left|i_{d1}^* - i_{d2}(k+2)\right| + \left|i_{q1}^* - i_{q1}(k+2)\right| \\ &+ \left|i_{d3}^* - i_{d3}(k+2)\right| + \left|i_{q3}^* - i_{q3}(k+2)\right| \end{aligned} \quad (8)$$

where "*" denotes the reference value. i={1,2,…,15}. Since the elements in the cost function have the same property essentially, it is unnecessary to use the weighting factor to connect different parts.

C. Reference Current Criterion

Under OCF situations, the reference current of the fundamental subspace is identical to that under the normal operation while the criteria for reference harmonic current are selected according to different requirements of drive applications. As mentioned previously, there are two control approaches for harmonic current tracking, namely, minimum loss and maximum torque.

1) Minimum loss

The ML criterion can maintain the overall faulty drive losses at the normal level, resulting in the unequal amplitudes of the remained phase currents and reduced output torque. If an open-phase fault occurs in phase A, the amplitude of phases C and D currents is the same, being larger than those of phases B and E. According to this criterion, the y-axis current becomes zero and the x-axis current is fixed to $-i_\alpha^*$, as expressed in (9).

$$\begin{cases} i_x^* = -i_\alpha^* \\ i_y^* = 0 \end{cases} \quad (9)$$

The current references in the d_3-q_3 reference frame can be derived using Park transformation as

$$\begin{cases} i_{d3}^* = -\left(i_{d1}^*\cos\theta - i_{q1}^*\sin\theta\right)\cos 3\theta \\ i_{q3}^* = \left(i_{d1}^*\cos\theta - i_{q1}^*\sin\theta\right)\sin 3\theta \end{cases} \quad (10)$$

2) Maximum torque

The MT principle is to ensure the torque output remains the same value as before a failure. As a result, the magnitude of healthy phase current is increased equally by a factor of 1.382. According to the result in [6], the current references in the x-y plane are presented as

$$\begin{cases} i_x^* = -i_\alpha^* \\ i_y^* = -0.2631 i_\beta^* \end{cases} \quad (11)$$

Similarly, the references of d_3-current and q_3-current are

$$\begin{cases} i_{d3}^* = -\left(i_{d1}^*\cos\theta - i_{q1}^*\sin\theta\right)\cos 3\theta - 0.2631\left(i_{d1}^*\sin\theta + i_{q1}^*\cos\theta\right)\sin 3\theta \\ i_{q3}^* = -\left(i_{d1}^*\cos\theta - i_{q1}^*\sin\theta\right)\sin 3\theta - 0.2631\left(i_{d1}^*\sin\theta + i_{q1}^*\cos\theta\right)\cos 3\theta \end{cases} \quad (12)$$

IV. MPTC For A Five-Phase PMSM Under OCF Condition

Similar to the fault-tolerant MPCC, when the MPTC method is applied in the fault-tolerant multi-phase drive, appropriate variables in fundamental and harmonic subspaces should be taken into consideration as a whole. In this study, apart from the torque and stator flux-linkage, the *x-y* currents are selected as a pair of additional control variables to realize the regulation of the *x-y* subspace. Fig. 4 illustrates the overall control structure of MPTC for the fault-tolerant five-phase PMSM drive.

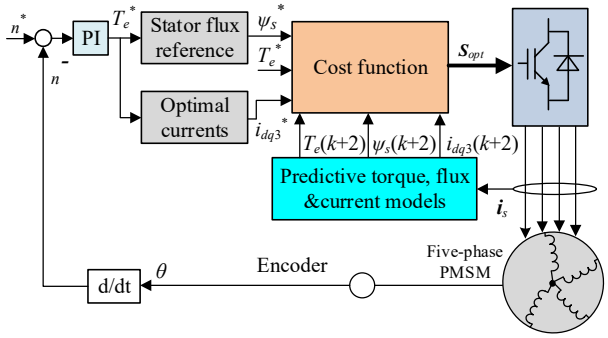

Fig. 4 Control diagram of fault-tolerant MPTC strategy for a five-phase PMSM under OCF condition.

A. Predictive Model

Based on the selected control variables (torque, stator flux, and the harmonic currents), the predictive models are constructed as follows

$$\begin{cases} i_{d3}(k+2)=(1-R_sT_s/L_{d3})i_{d3}(k+1)+3\omega_eT_sL_{q3}i_{q3}(k+1)/L_{d3}+T_sv_{d3}/L_{d3} \\ i_{q3}(k+2)=(1-R_sT_s/L_{q3})i_{q3}(k+1)-3\omega_eT_sL_{d3}i_{d3}(k+1)/L_{q3}+T_sv_{q3}/L_{q3} \end{cases} \quad (13)$$

$$\begin{cases} \psi_{sd}(k+2)=L_{d1}i_{d1}(k+2)+\psi_f \\ \psi_{sq}(k+2)=L_{q1}i_{q1}(k+2) \end{cases} \quad (14)$$

$$T_e(k+2)=\frac{5}{2}P_r\left[\psi_f i_{q1}(k+2)+(L_{d1}-L_{q1})i_{d1}(k+2)i_{q1}(k+2)\right] +3(L_{d3}-L_{q3})i_{d3}(k+2)i_{q3}(k+2) \quad (15)$$

B. Cost Function

In order to achieve the best switching state, a cost function is constructed by using the absolute errors of the control objectives, where two weighting factors are required to balance the importance of three control variables due to differing natures. Finally, the cost function is defined as

$$g_i=\left|T_e^*-T_e(k+2)\right|+\lambda_1\left[\left|\psi_{sd}-\psi_{sd}(k+2)\right|+\left|\psi_{sq}^*-\psi_{sq}(k+2)\right|\right] +\lambda_2\left[\left|i_{d3}^*-i_{d3}(k+2)\right|+\left|i_{d3}^*-i_{d3}(k+2)\right|\right] \quad (16)$$

The reference torque is the output of the speed controller. Due to the similar inductance components in the *d-q* plane, the control method i_{d1}=0 can be considered as the maximum torque per ampere and used to reduce the stator copper loss. Besides, i_{q1}^* which is proportional to the reference torque is expressed as

$$i_{q1}^*=2T_e^*/(5P_r\psi_f) \quad (17)$$

Consequently, the stator flux reference can be obtained as

$$\begin{cases} \psi_{sd}^*=L_{d1}i_{d1}^*+\psi_f \\ \psi_{sq}^*=L_{q1}i_{q1}^* \end{cases} \quad (18)$$

V. Relation of Two MPC Methods

Since three control variables with different natures are employed, the predictive model of the fault-tolerant MPTC, expressed by equations (13)-(15), is relatively complicated when compared with equation (7) for the fault-tolerant MPCC. Noticeably, one identity in two predictive models is that the d_3q_3-axes currents are predicted.

Apart from the predictive model, differences and similarities can be found with the cost function. Considering i_{d1}=0 control method and the similar inductances in the *d-q* axis, the cost function in (8) is rewritten as

$$c_i=c_1+c_2+c_3+c_4 \quad (19)$$

where,

$$c_1=\left|i_{d1}(k+2)\right|,\ c_2=\left|i_{q1}^*-i_{q1}(k+2)\right|,\ c_3=\left|i_{d3}^*-i_{d3}(k+2)\right|$$
$$c_3=\left|i_{q3}^*-i_{q3}(k+2)\right|$$

Likewise, the cost function of MPTC can be expressed as

$$g_i=g_1+g_2+g_3 \quad (20)$$

where,

$$g_1=|T_e^*-5P_r\psi_f i_{q1}(k+2)/2|$$
$$g_2=\lambda_1[L_{d1}|i_{d1}(k+2)|+L_{q1}|i_{q1}^*-i_{q1}(k+2)|]$$
$$g_3=\lambda_2[|i_{d3}^*-i_{d3}(k+2)|+|i_{q3}^*-i_{q3}(k+2)|]$$

According to equations (19) and (20), the following relationships can be directly concluded as

$$g_1=(5P_r\psi_f/2)c_2 \quad (21)$$
$$g_2=\lambda_1(L_{d1}c_1+L_{q1}c_2) \quad (22)$$
$$g_3=\lambda_2(c_3+c_4) \quad (23)$$

Consequently, the cost function of MPTC can be further modified as

$$g_i=\mu_1c_1++\mu_2c_2+\mu_3(c_3+c_4) \quad (24)$$

where

$$\mu_1=\lambda_1L_{d1},\ \mu_2=\lambda_1L_{q1}+5P_r\psi_f/2,\ \mu_3=\lambda_2$$

The newly obtained function in (24) has clearly demonstrated the link between fault-tolerant MPCC and MPTC. In essence, the optimization process of both MPC methods can be implemented in terms of predicted currents and outputs of speed regulators. Specifically, the current prediction in two methods is identical. The output of the speed controller in MPTC is proportional to that in MPCC. Since there is no inner loop, the transient response is dependent on the bandwidth of the speed controller. In addition, the system behavior by fault-tolerant MPTC is highly associated with two weighting factors.

For the desired weighting factors, the ratio λ_{1n} between the rated values of the torque and stator flux-linkage is considered and set as a benchmark. Meanwhile, the ratio λ_{2n} between the nominal amplitudes of the torque and harmonic current is set as another benchmark [19]. The definitions are expressed by equations (25)-(28). Then, standard deviations of the d_1q_1-currents and *y*-current are calculated to evaluate performances by different weighting factors around the benchmarks. With these quantitative analyses, the best weighting factors can be

achieved.

$$\lambda_{1n}=T_{en}/\psi_{sn} \tag{25}$$

$$\lambda_{2n}=T_{en}/i_{fn} \tag{26}$$

$$\psi_{sn}=\sqrt{\psi_f^2+[2T_{en}L_{q1}/(5P_r\psi_f)]^2} \tag{27}$$

$$i_{fn}=\sqrt{i_{xn}^2+i_{yn}^2}=i_{\alpha n}=2T_{en}/(5P_r\psi_f) \tag{28}$$

where T_{en} is rated torque. ψ_{sn} and i_{fn} are nominal magnitudes of stator flux-linkage and harmonic current. i_{xn}, i_{yn} and $i_{\alpha n}$ is the nominal magnitude of x-, y- and α-axis currents, respectively.

Substituting the nominal values (listed in Table I) into (25)-(26), the benchmarks are 458.72 and 1.58 with respect to λ_{1n} and λ_{2n}. Thereafter, applying the benchmarks into (24), the following equation can be obtained as

$$g_i = 1.15c_1+2.91c_2+1.58(c_3+c_4) \tag{29}$$

Compared to the cost function of MPCC in (20), the coefficient of each component is increased. The maximum gain is found with the q_1-axis current.

TABLE I
KEY PARAMETERS OF THE FIVE-PHASE PMSM

Items	Specifications
No. of poles in rotor	18
Phase resistance	0.3 Ω
d_1-axis inductance	2.5 mH
q_1-axis inductance	2.9 mH
d_3-axis inductance	2.5 mH
q_3-axis inductance	2.5 mH
PM flux-linkage	0.035 Wb
Rated torque	30 Nm

VI. Simulations

To assess the performance of the fault-tolerant MPC and MPTC methods for a five-phase PMSM drive under OCF conditions, simulations are conducted in the environment of MATLAB/Simulink. The key parameters of the five-phase PMSM are the same as those in the experimental setup, which are shown in Table I.

A. Relation Discussion

In the previous section, the relation between the fault-tolerant MPCC and MPTC is analyzed through the cost function, as presented in (24) and (29). For the purpose of quantitative evaluation, the total harmonic distortion (THD) and the torque ripple are employed as two evaluating indicators. Since μ_1 is closed to 1 in (29), this variable is fixed to 1 in simulations. Fig. 5 shows the evaluation results of the phase A current and the torque by the fault-tolerant MPCC with different coefficients. The reference speed is 800rpm with a load of 20Nm. The dark blue block indicates a low THD value and a low torque ripple. When μ_1 and μ_2 are equal to 1, the cost function in (24) is equivalent to that of the fault-tolerant MPCC. As shown in Fig. 5, the phase currents are desirable with low THD values while the torque ripple is not minimized. When μ_2 is in the range from 2 to 4 and μ_3 increases to a value of 2, the lower torque ripple can be obtained and the THD is nearly changed. Consider the expression in (29), it can be concluded that the benchmarks of the weighting factors can theoretically improve the torque performance of the fault-tolerant MPTC.

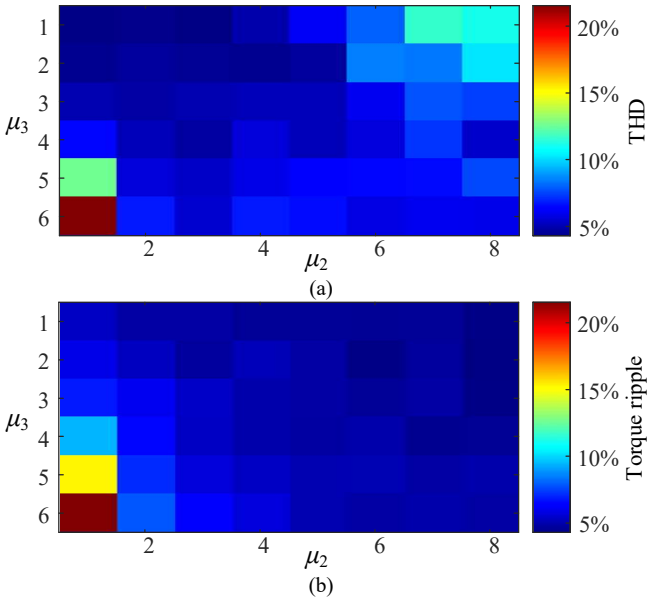

Fig. 5 Evaluations of simulated current and torque by MPCC with different coefficients. (a) THD. (b) torque ripples.

B. Weighting Factor Tuning

The impact of two weighting factors in the fault-tolerant MPTC on system behavior has been investigated by repetitive simulations. For the sake of simplification, the ML principle is employed, where the reference of the y-axis current is constant. Fig. 6 illustrates the standard deviations of the y-axis current by fault-tolerant MPTC with different weighting factors. According to the above-mentioned benchmarks, the sweeping ranges of λ_1 and λ_2 are from 0 to 4000 and from 0 to 5, respectively. As shown in Fig. 6, the darker regions indicate a good performance of currents. Consequently, the ranges of two weighting factors are finally obtained as $800\leq\lambda_1\leq1200$ and $0.8\leq\lambda_2\leq4$.

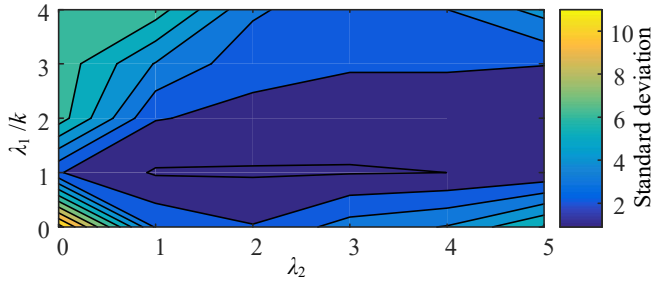

Fig. 6 Standard deviations of simulated y-axis current by MPTC with different weighting factors.

C. Condition Transitions

Fig. 7 demonstrates the transitions from the normal to the fault-tolerant operations by two MPC methods with both the ML and MT criteria. The best value of weighting factors λ_1 and λ_2 are specified as 500 and 1.7, respectively. Accordingly, the values of the two coefficients μ_2 and μ_3 are 3.02 and 1.7, respectively, which belong to the above-mentioned ranges. Compared with the fault-tolerant MPCC, the fault-tolerant

MPTC with the optimal weighting factors is supposed to suppress torque ripple.

Under the healthy situation, the virtual vector (VV) presented in [31] is used in conjunction with the MPCC and MPTC. The phase currents are balanced and sinusoidal with the harmonic current being well suppressed, as shown in Figs. 7(a) and 7(b). At the instant t=0.01s, an open-phase fault occurs in phase A. Accordingly, the phase A current becomes null and the currents in the healthy phases vary irregularly. Besides, the magnitudes of the x-y currents, the torque ripple and the copper loss increase significantly. When t=0.03s, the fault-tolerant MPC with the ML principle is applied. The remaining phase currents become balanced, where the amplitudes of the currents in phases B and E are the same and higher than those in phases C and D. In addition, the y-axis current is nearly null and the copper loss decreases. The torque ripple is also suppressed although it is relatively higher than that in the normal state. Once the ML method is replaced by the MT, the amplitudes of phase currents become equal and y-current increases immediately, which is consistent with the theoretical analysis. Meanwhile, the average value of the copper loss rises, as listed in Table II. Since the load torque is less than the maximum achievable value, the average torque output is the same under the ML and MT modes [32].

In summary, the open-phase fault would increase harmonic currents, torque ripples as well as copper losses. The VV-based MPC cannot maintain the faulty system performance at the pre-fault level. Although the simulated waveforms of two fault-tolerant methods during transitions are quite similar, they verify that both schemes can address the failure and ensure the fault-tolerant operation of the drive. In contrast with the MT, the ML can suppress the system loss. Hence, to reduce the overall drive loss in the post-fault operation, the ML method should be applied when the phase currents are below the rated value, while the MT method would be used if the demanded torque is required. Moreover, the fault-tolerant MPTC generates a lower torque ripple, which agrees with the analysis in Section VI-B. This is mainly because that the more desirable coefficient of each current component in the cost function is applied.

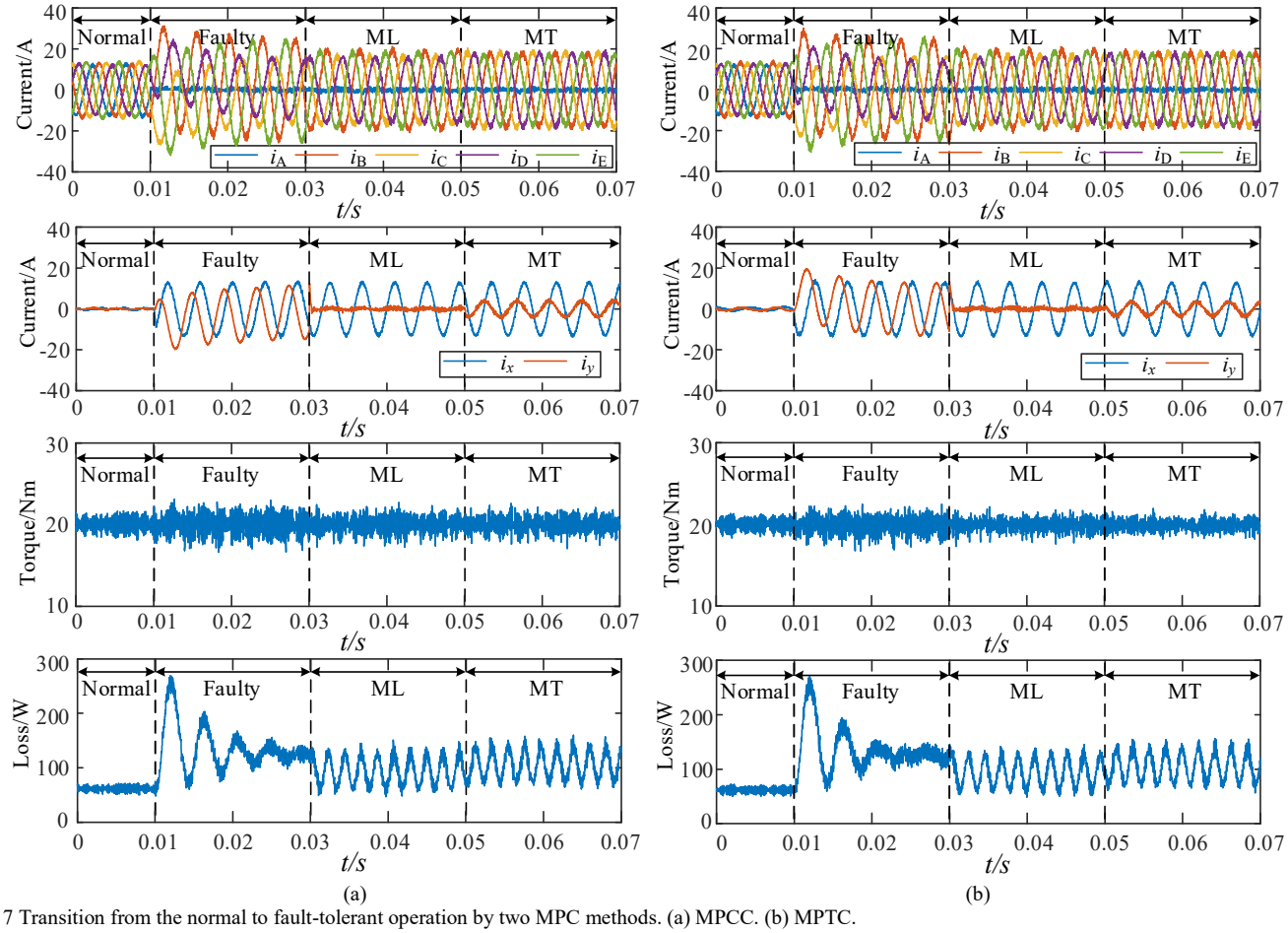

Fig. 7 Transition from the normal to fault-tolerant operation by two MPC methods. (a) MPCC. (b) MPTC.

TABLE II
SIMULATED PERFORMANCE EVALUATIONS FOR TWO FAULT-TOLERANT MPC METHODS

Items	VV-MPCC		Fault-tolerant MPCC		VV-MPTC		Fault-tolerant MPTC	
	Normal	Faulty	ML	MT	Normal	Faulty	ML	MT
Torque ripple (%)	4.52	6.33	5.57	5.22	3.64	5.76	4.13	4.02
Copper loss (W)	61.10	128.13	94.30	105.60	61.24	124.38	93.23	104.88

VII. EXPERIMENTS

To further evaluate two fault-tolerant MPC approaches, experimental validations are carried out on a five-phase PMSM. The experimental platform is shown in Fig. 8. The five-phase PMSM is coupled mechanically with a magnetic powder brake, which is used to provide load torques. The five-phase inverter is built using five power modules (FF300R12ME4) with drivers of 2SP0115T. The phase current and DC-link voltage are measured by LEM current sensor and LEM voltage transducer, respectively. The actual rotor position is obtained by an incremental encoder with 2000 pulses per revolution. The control algorithm is implemented in a DSP-TMS320F28335 control board. Phase currents are captured and displayed by an oscilloscope. The other variables which cannot be directly acquired are recorded by the memory of DSP and then processed in Matlab.

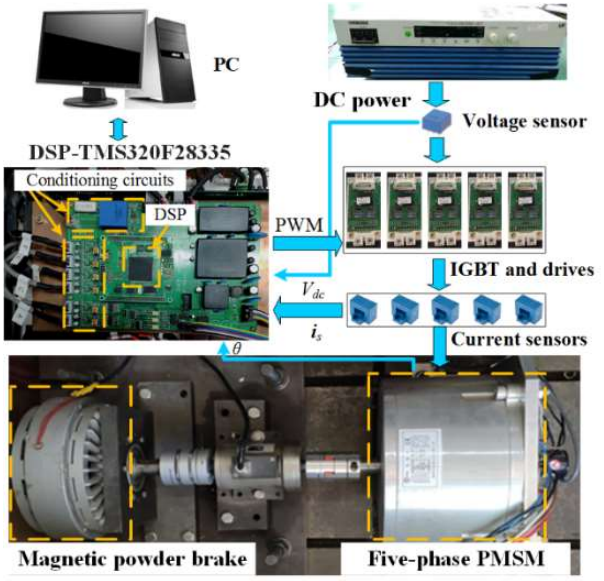

Fig. 8 Experimental platform.

A. Steady-State Performance

The steady-state test is performed to assess the behaviors by MPCC and MPTC with both ML and MT criteria. The execution time of the main MPC modular is 44.22us and 62.15us with respect to MPCC and MPTC. Obviously, the computational cost of MPTC is relatively higher than MPCC. The main reason is that the estimation and prediction of both torque and stator flux-linkage increase computational workload. The sampling frequency is set to 12kHz for both MPC methods. The five-phase system is driven at 300 rpm with a load of 15Nm. According to the results in Fig. 6, the weighting factors λ_1 and λ_2 in the fault-tolerant MPTC are specified to 800 and 1, respectively. To guarantee a fair comparison, the same parameters are used for speed PI controllers in two MPC methods. The OCFs in phase A are implemented by turning off the driving signal of the corresponding switches.

Fig. 9 exhibits the steady-state phase currents, *x-y* currents, and torque waveforms by two MPC methods. It can be seen that the fundamental and harmonic subspaces are well regulated. As stated earlier, the ML principle results in the unequal amplitudes of four-phase currents. By contrast, the amplitudes of four-phase currents by MT are equal. Quantitative evaluations of phase currents by two MPC methods are illustrated in Fig. 10. From Fig. 10(a), it is found that THD values of phase currents by MPCC are almost lower than those by MPTC. This is mainly because that the importance of different current components is well balanced in the cost function of MPCC. However, the amplitudes of currents by two MPC methods are similar regardless of the criterion for harmonic current, as shown in Fig. 10(b). It should be mentioned that due to the asymmetry of the five-phase windings of the PMSM caused by the manufacture, the measured current in phase C is slightly larger than others in magnitude. Consequently, it can be concluded that the MPCC outperforms MPTC in phase current performance.

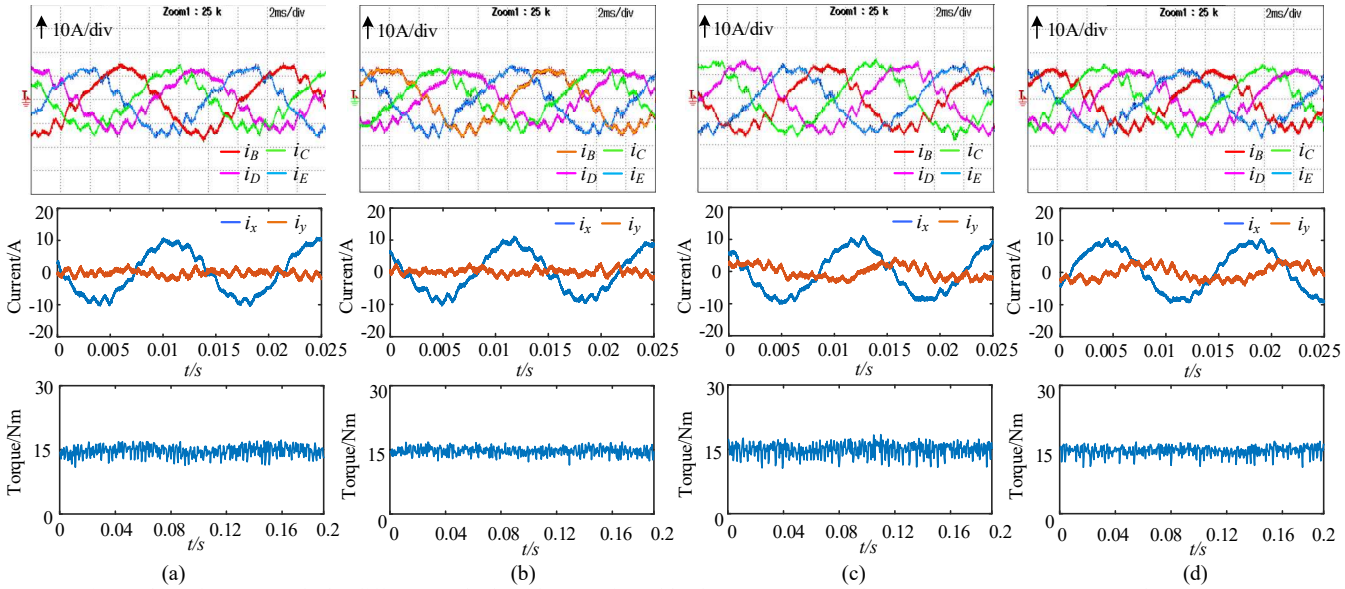

Fig. 9 Experimental steady-state results by different methods with 50% of rated load. (a) MPCC-ML. (b) MPTC-ML. (c) MPCC-MT. (d) MPTC-MT.

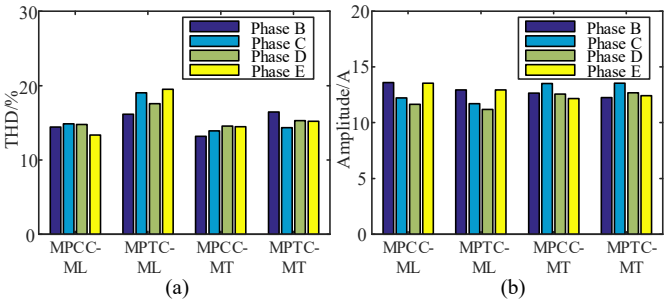

Fig. 10 Evaluations of phase currents by two MPC methods. (a) THD. (b) Amplitude.

Table III shows the detailed torque performance. The average torque of MPCC-ML, MPTC-ML, MPCC-MT, and MPTC-MT is 14.90Nm, 14.95Nm, 14.96Nm, and 14.92Nm, respectively, which means the average torque in the ML mode is quite similar to that in the MT mode, since the output torque has not reached the torque/current limitation [20]. The torque ripple is 8.47%, 6.66%, 10.07%, and 7.60% with respect to MPCC-ML, MPTC-ML, MPCC-MT, and MPTC-MT, which reveals that MPTC can reduce torque pulsations compared to its counterpart. The reason may lie in the fact that the importance of the q_1-axis current component is increased in the cost function of MPTC.

In addition, the switching frequency analyses in Table III illustrate that the average switching frequency of MPTC is higher than that of MPCC. As for two criteria for harmonic current, a higher average switching frequency is found with ML.

B. Condition Transition

To further explore the fault-tolerance of MPCC and MPTC, the transition tests are conducted from the faulty condition to the fault-tolerant condition. Similar to the simulations, the VV algorithm is applied in the MPCC and MPTC. After OCF, the five-phase drive operates in the post-fault condition initially while the control strategy remains unchanged. As shown in Fig. 11, when the faulty drive operates with the healthy MPC methods, the currents in the α-β and x-y subspaces are similar to those by fault-tolerant MPC with ML principle [Figs. 8(a) and 7(c)]. The detailed analyses in Table IV indicate that both VV-based MPC methods can almost provide desirable average torque. Nevertheless, the torque ripples are considerable, which are 13.64% and 11.78% with respect to the VV-based MPCC and the VV-based MPTC. It can be concluded that the five-phase PMSM drive cannot maintain a similar performance after OCF.

TABLE III
STEADY-STATE PERFORMANCE ASSESSMENTS FOR TWO MPC METHODS

Items	MPCC		MPTC	
	ML	MT	ML	MT
Average torque (Nm)	14.90	14.96	14.95	14.92
Torque ripple (%)	8.47	10.07	6.66	7.60
Average switching frequency (kHz)	2.00	1.79	2.57	2.19

For better illustration, the MT criterion is used in conjunction with fault-tolerant MPCC and MPTC. When the fault-tolerant MPC schemes are applied, the currents vary as expected and the torque ripples decrease to 8.60% and 7.35% with respect to MPCC and MPTC. Being identical with the results of the steady-state test, MPTC methods can offer relatively lower torque pulsation. The transition test shows that both fault-tolerant MPC methods can address OCF effectively and provide similar performances as before OCF.

TABLE IV
TRANSITION PERFORMANCE ASSESSMENTS FOR DIFFERENT MPC METHODS

Items	VV-MPCC	VV-MPTC	MPCC	MPTC
THD of current (%)	17.18	19.21	13.83	16.16
Average torque (Nm)	14.92	15.00	15.01	15.02
Torque ripple (%)	13.64	11.78	8.60	7.35

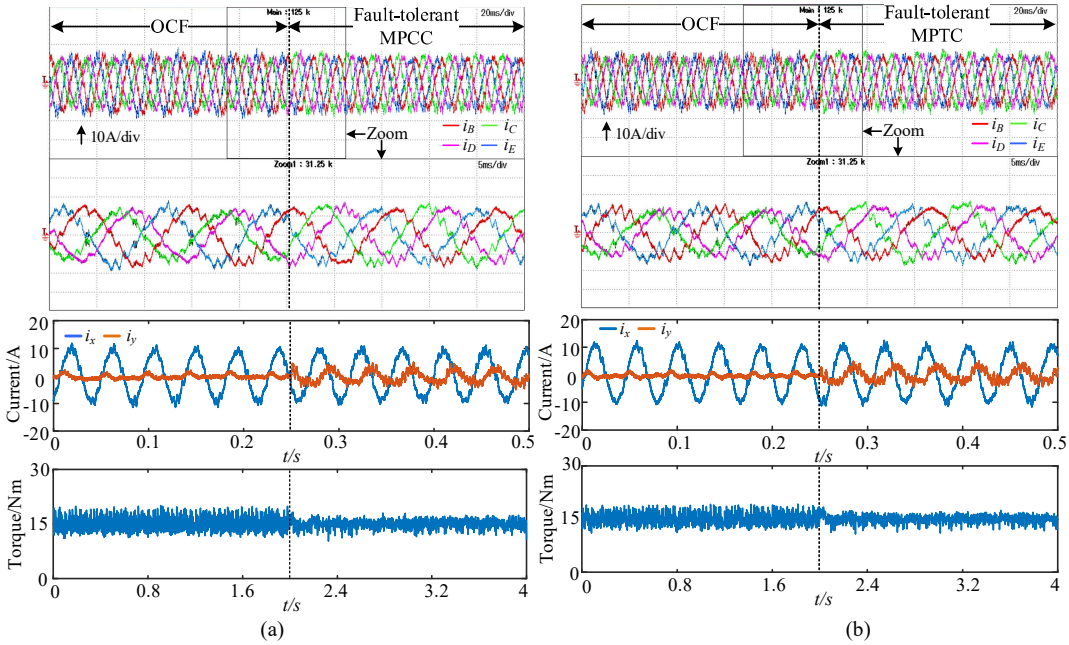

Fig. 11 Transition from OCF condition to fault-tolerant operation by two MPC methods. (a) MPCC-MT. (b) MPTC-MT

C. Dynamic Performance

Apart from the steady-state and the transition tests, the dynamic experiment is also conducted. Fig. 12 shows speed reversal behaviors by MPCC-MT and MPTC-MT. When t=0.4s, the speed reference varies from 300rpm to -300rpm with a constant load of 15Nm. To achieve the same limit of the current and the torque for two MPC methods, the linear relationship between the q_1-current and the torque is used. The output limit of the PI controller in MPCC is specified to ±20A. According to (17), the limit in MPTC is ±31.5Nm. When the speed reference changes, the torque outputs reach the lower limit (-31.5Nm). Besides, the speed response is quantitatively assessed by using the function of stepinfo in MATLAB [33]. The settling time of the speed (0.19s) in MPCC is close to that in MPTC (0.18s).

Fig. 13 demonstrates the experimental results by two methods with MT under load variation conditions. When the faulty drive operates under the steady-state of 300rpm without load, an external load of 15Nm is added suddenly at the instant of 0.4s. After the load step, a small drop of the speed (around 20rpm) can be seen with both MPCC and MPTC. It takes 0.15s for each speed to recover to the reference. Meanwhile, it can be seen that the response by two fault-tolerant approaches is quite similar.

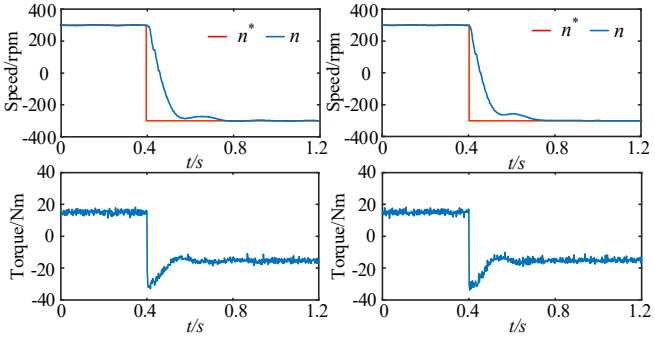

Fig. 12 Speed reversal test by two fault-tolerant MPC methods. (a) MPCC-MT. (b) MPTC-MT.

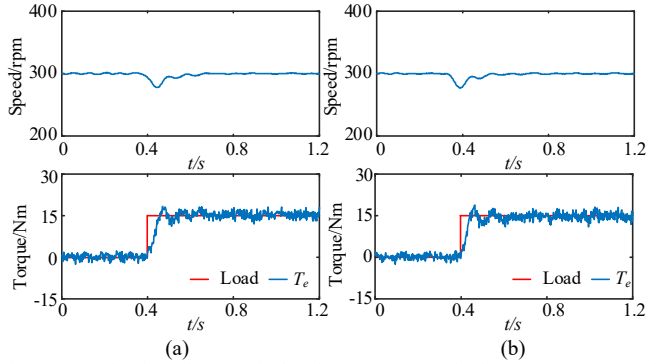

Fig. 13 Step load test by two fault-tolerant MPC methods. (a) MPCC-MT. (b) MPTC-MT.

The tests above reveal that the transient behavior by MPCC is highly analogous to that by MPTC. This result can be explained by the employment of the same parameters of PI-based speed regulator. In addition, the dynamic response capability of the MPC-controlled drive system is dependent on the bandwidth of the speed controller.

VIII. Conclusion

The fault-tolerant MPCC and MPTC have been explored for a five-phase PMSM drive under OCF operation. The relationship between two methods is investigated through cost functions. Besides, the performance of two methods is evaluated in terms of steady-state, transition, and dynamic tests. According to the quantitative comparisons, the conclusions are drawn as

1) Both MPCC and MPTC can address OCF effectively.

2) The number of the control variables in MPTC is more than that in MPCC. The increased control variables lead to more predictions and constraints, resulting in larger computation.

3) Two weighting factors are used for the cost function of MPTC to balance the importance of different variables. The inappropriate weighting factor has an adverse impact on the system performance. While the weighting factor is not required in MPCC.

4) MPCC is superior to MPTC in current performance since the importance of current components in the cost function is well balanced, while MPTC offers a lower torque ripple due to the increased weight of q_1-axis current.

5) The transient performances of two fault-tolerant MPC methods are similar when the same speed controller is applied.

6) The optimization process of both MPC schemes is dependent on the current prediction and the output of the speed controller.

Summarily, this work can provide effective guidance for the MPC method selection for fault-tolerant control of multiphase drives under OCF conditions.

References

[1] E. Levi, "Multiphase Electric Machines for Variable-Speed Applications," *IEEE Trans. Ind. Electron.*, vol. 55, no. 5, pp. 1893-1909, May 2008.

[2] F. Barrero and M. J. Duran, "Recent Advances in the Design, Modeling, and Control of Multiphase Machines—Part I," *IEEE Trans. Ind. Electron.*, vol. 63, no. 1, pp. 449-458, Jan. 2016.

[3] Z. Liu, Y. Li and Z. Zheng, "A review of drive techniques for multiphase machines," *CES Transactions on Electrical Machines and Systems*, vol. 2, no. 2, pp. 243-251, Jun. 2018.

[4] L. Parsa and H. A. Toliyat, "Five-phase permanent-magnet motor drives," *IEEE Trans. Ind. Appl.*, vol. 41, no. 1, pp. 30-37, Jan.-Feb. 2005.

[5] Z. Wang, X. Wang, Y. Wang, J. Chen and M. Cheng, "Fault tolerant control of multiphase multilevel motor drives - technical review," *Chinese Journal of Electrical Engineering*, vol. 3, no. 2, pp. 76-86, Sep. 2017.

[6] M. J. Duran and F. Barrero, "Recent advances in the design, modeling, and control of multiphase machines -Part II," *IEEE Trans. Ind. Electron.*, vol. 63, no. 1, pp. 459-468, Jan. 2016.

[7] S. Dwari and L. Parsa, "An Optimal Control Technique for Multiphase PM Machines Under Open-Circuit Faults," *IEEE Trans. Ind. Electron.*, vol. 55, no. 5, pp. 1988-1995, May 2008.

[8] G. Liu, L. Qu, W. Zhao, Q. Chen and Y. Xie, "Comparison of Two SVPWM Control Strategies of Five-Phase Fault-Tolerant Permanent-Magnet Motor," *IEEE Trans. Power Electron.*, vol. 31, no. 9, pp. 6621-6630, Sept. 2016.

[9] G. Liu, Z. Lin, W. Zhao, Q. Chen and G. Xu, "Third harmonic current injection in fault-tolerant five-phase permanent-magnet motor drive," *IEEE Trans. Power Electron*., vol. 33, no. 8, pp. 6970-6979, Aug. 2018.

[10] M. Bermudez, I. Gonzalez-Prieto, F. Barrero, H. Guzman, M. J. Duran and X. Kestelyn, "Open-phase fault-tolerant direct torque control technique for five-phase induction motor drives," *IEEE Trans. Ind. Electron.*, vol. 64, no. 2, pp. 902-911, Feb. 2017.

[11] L. Zhang, Y. Fan, R. Cui, R. D. Lorenz and M. Cheng, "Fault-tolerant

direct torque control of five-phase FTFSCW-IPM motor based on analogous three-phase SVPWM for electric vehicle applications," *IEEE Trans. Veh. Technol.*, vol. 67, no. 2, pp. 910-919, Feb. 2018.

[12] Y. Zhou, X. Lin and M. Cheng, "A Fault-Tolerant Direct Torque Control for Six-Phase Permanent Magnet Synchronous Motor with Arbitrary Two Opened Phases Based on Modified Variables," *IEEE Trans. Energy Convers.*, vol. 31, no. 2, pp. 549-556, June 2016.

[13] Z. Wang, X. Wang, J. Cao, M. Cheng and Y. Hu, "Direct torque control of T-NPC inverters-fed double-stator-winding PMSM drives with SVM," *IEEE Trans. Power Electron.*, vol. 33, no. 2, pp. 1541-1553, Feb. 2018.

[14] S. Vazquez, J. Rodriguez, M. Rivera, L. G. Franquelo and M. Norambuena, "Model Predictive Control for Power Converters and Drives: Advances and Trends," *IEEE Trans. Ind. Electron.*, vol. 64, no. 2, pp. 935-947, Feb. 2017.

[15] M. Cheng, F. Yu, K. T. Chau and W. Hua, "Dynamic Performance Evaluation of a Nine-Phase Flux-Switching Permanent-Magnet Motor Drive with Model Predictive Control," *IEEE Trans. Ind. Electron.*, vol. 63, no. 7, pp. 4539-4549, July 2016.

[16] X. An, G. Liu, Q. Chen, W. Zhao and X. Song, "Robust Predictive Current Control for Fault-Tolerant Operation of Five-Phase PM Motors Based on Online Stator Inductance Identification," *IEEE Trans. Power Electron.*, early access, to be published, 2021, doi: 10.1109/TPEL.2021.3077235.

[17] W. Huang, W. Hua, F. Chen, F. Yin and J. Qi, "Model predictive current control of open-circuit fault-tolerant five-phase flux-switching permanent magnet motor drives," *IEEE J. Emerging Sel. Topics Power Electron.*, vol. 6, no. 4, pp. 1840-1849, Dec. 2018.

[18] Y. Zhang and H. Yang, "Model Predictive Torque Control of Induction Motor Drives with Optimal Duty Cycle Control," *IEEE Trans. Power Electron.*, vol. 29, no. 12, pp. 6593-6603, Dec. 2014.

[19] J. Rodriguez, R. M. Kennel, J. R. Espinoza, M. Trincado, C. A. Silva and C. A. Rojas, "High-Performance Control Strategies for Electrical Drives: An Experimental Assessment," *IEEE Trans. Ind. Electron.*, vol. 59, no. 2, pp. 812-820, Feb. 2012.

[20] W. Zhao, H. Wang, T. Tao and D. Xu, "Model Predictive Torque Control of Five-Phase PMSM by Using Double Virtual Voltage Vectors Based on Geometric Principle," *IEEE Trans. Transp. Electr.*, early access, to be published, 2021, doi: 10.1109/TTE.2021.3063193.

[21] H. Guzman et al., "Comparative study of predictive and resonant controllers in fault-tolerant five-phase induction motor drives," *IEEE Trans. Ind. Electron.*, vol. 63, no. 1, pp. 606-617, Jan. 2016.

[22] H. Lu, J. Li, R. Qu, D. Ye and Y. Lu, "Fault-Tolerant Predictive Control of Six-Phase PMSM Drives Based on Pulsewidth Modulation," *IEEE Trans. Ind. Electron.*, vol. 66, no. 7, pp. 4992-5003, July 2019.

[23] Y. Luo and C. Liu, "Pre- and Post-Fault Tolerant Operation of a Six-Phase PMSM Motor Using FCS-MPC Without Controller Reconfiguration," *IEEE Trans. Veh. Technol.*, vol. 68, no. 1, pp. 254-263, Jan. 2019.

[24] Y. Zhou and G. Chen, "Predictive DTC Strategy with Fault-Tolerant Function for Six-Phase and Three-Phase PMSM Series-Connected Drive System," *IEEE Trans. Ind. Electron.*, vol. 65, no. 11, pp. 9101-9112, Nov. 2018.

[25] W. Huang, W. Hua, F. Chen, M. Hu and J. Zhu, "Model Predictive Torque Control with SVM for Five-Phase PMSM under Open-Circuit Fault Condition," *IEEE Trans. Power Electron.*, vol. 35, no. 5, pp. 5531-5540, May 2020.

[26] W. Huang, W. Hua, F. Chen and J. Zhu, "Enhanced Model Predictive Torque Control of Fault-Tolerant Five-Phase Permanent Magnet Synchronous Motor with Harmonic Restraint and Voltage Preselection," *IEEE Trans. Ind. Electron.*, vol. 67, no. 8, pp. 6259-6269, Aug. 2020.

[27] M. Bermudez, I. Gonzalez-Prieto, F. Barrero, H. Guzman, X. Kestelyn and M. J. Duran, "An Experimental Assessment of Open-Phase Fault-Tolerant Virtual-Vector-Based Direct Torque Control in Five-Phase Induction Motor Drives," *IEEE Trans. Power Electron.*, vol. 33, no. 3, pp. 2774-2784, March 2018.

[28] J. Scoltock, T. Geyer and U. K. Madawala, "A Comparison of Model Predictive Control Schemes for MV Induction Motor Drives," *IEEE Trans. Ind. Inform.*, vol. 9, no. 2, pp. 909-919, May 2013.

[29] F. Wang, S. Li, X. Mei, W. Xie, J. Rodríguez and R. M. Kennel, "Model-Based Predictive Direct Control Strategies for Electrical Drives: An Experimental Evaluation of PTC and PCC Methods," *IEEE Trans. Ind. Electron.*, vol. 11, no. 3, pp. 671-681, June 2015.

[30] M. Siami, D. A. Khaburi, M. Rivera and J. Rodríguez, "An Experimental Evaluation of Predictive Current Control and Predictive Torque Control for a PMSM Fed by a Matrix Converter," *IEEE Trans. Ind. Electron.*, vol. 64, no. 11, pp. 8459-8471, Nov. 2017.

[31] W. Hua, F. Chen, W. Huang, G. Zhang, W. Wang and W. Xia, "Multivector-Based Model Predictive Control With Geometric Solution of a Five-Phase Flux-Switching Permanent Magnet Motor," *IEEE Trans. Ind. Electron.*, vol. 67, no. 12, pp. 10035-10045, Dec. 2020.

[32] H. Guzman, M. J. Duran, F. Barrero, B. Bogado and S. Toral, "Speed Control of Five-Phase Induction Motors With Integrated Open-Phase Fault Operation Using Model-Based Predictive Current Control Techniques," *IEEE Trans. Ind. Electron.*, vol. 61, no. 9, pp. 4474-4484, Sept. 2014.

[33] MATLAB and System Identification Toolbox, MathWorks, Inc., Natick, Massachusetts, United States, 2015.

Wentao Huang received the Ph.D. degree in Electrical Engineering from Southeast University, Nanjing, China, in 2020. From January 2018 to January 2019, he was a joint-supervised Ph.D. student with the School of Electrical and Data Engineering, University of Technology Sydney, NSW, Australia.

Since 2020, he has been with Jiangnan University, Wuxi, China, where he is currently a Lecturer with the School of Internet of Things Engineering. His major research interests include permanent magnet machine drives, fault diagnosis and fault-tolerant control.

Wei Hua (M'03-SM'16) received B.Sc. and Ph.D. degrees both in Electrical Engineering from the School of Electrical Engineering, Southeast University, Nanjing, China, in 2001 and 2007, respectively. During 2004.9-2005.8, he visited the department of Electronics and Electrical Engineering, The University of Sheffield, U.K., as a joint-supervised Ph. D. student.

Since 2007, he has been with Southeast University, where he is currently a Chief Professor with the School of Electrical Engineering. He is the author or coauthor of over 140 technical papers, and he is the holder of 60 patents in his areas of interest. His teaching and research interests include the design, analysis, and control of electrical machines.

Qigao Fan received the Ph.D. degree in Mechatronic Engineering from the School of Mechatronic Engineering, China University of Mining Technology, Xuzhou, China, in 2013.

Since 2013, he has been with Jiangnan University, Wuxi, China, where he is currently an Associate Professor with the School of Internet of Things Engineering. From September 2018 to September 2019, he was a visiting scholar with the Department of Mechanical and Industrial Engineering, University of Toronto. His teaching and research interests include motor control, robotics, intelligent sensors, and IoT technology.